Galactic chemical evolution in hierarchical formation models

Arrigoni, Matias

Chapter 3

Abundance ratios and iron content of the Intracluster Medium.

Abstract

We use the cosmological semi-analytic model (SAM) for galaxy formation presented in Chapter 2 to study the metallicities and abundance ratios of the intracluster medium (ICM) within the hierarchical structure formation paradigm. By requiring a slightly flat IMF ($x = 1.15$) and a two-population delay-time-distribution (DTD) for SN Ia explosions we found previously that this model is able to reproduce the abundance ratios and supernova rates of early-type galaxies in the local Universe. Predictions for elemental abundances in the ICM pose a further test of the model. We find that with the fiducial model from Chapter 2 the overall metal content of the ICM is too low, although the abundance ratios are in good agreement with the data. However, we find that allowing a fraction of the metal-enriched material ejected by stars to be deposited directly into the hot ICM, instead of being deposited into the cold ISM, appears to be a plausible and physically-motivated solution.

based on Arrigoni M., Trager S.C. and Somerville R.S., 2010, submitted to MNRAS

3.1 Introduction

THE vast majority of baryons in the Universe reside not in stars but in the hot and diffuse gas in clusters of galaxies—the intracluster medium (ICM)—part of which cools down onto galaxies providing the fuel for star formation (e.g. Lin et al. 2003; Vikhlinin et al. 2006). The metal content in this gas suggests that it cannot be entirely of primordial origin and that a substantial fraction must have been processed by the cluster galaxies and then expelled back into the ICM via supernovae explosions and galactic winds. This interplay between the ICM and galaxies regulates the star formation and enrichment histories (Renzini 1997) of the Universe. Measurement of elemental abundances in clusters can therefore set constraints on the various feedback processes that shape galaxy formation, as well as the relative importance of different types of supernovae and the history of star formation. Any successful model of galaxy formation must account not only for the observational properties of the galaxy population but also those of the ICM.

The intergalactic medium within groups and clusters is hot and dense enough to be observed at X-ray wavelengths. At these wavelengths Fe is the most easily observable element. The X-ray satellites launched since the mid-90's (ASCA, BeppoSax, Chandra, XMM-Newton, Suzaku) have allowed precise measurements of many other elements such as O, Mg, Si, S, Ar, Ca and Ni in large samples of nearby clusters (Fukazawa et al. 1998; Peterson et al. 2003; De Grandi et al. 2004; Tamura et al. 2004; de Plaa et al. 2007). The dominant process considered for the pollution of the ICM is the outflows of enriched gas in supernova-driven galactic winds (White 1991; Renzini 1997). There are, however, other sources that may have a non-negligible contribution to the metal enrichment of the ICM, such as hypernovae associated with population type III stars (Loewenstein 2001), intra-cluster stars (Zaritsky et al. 2004; Murante et al. 2007; Sivanandam et al. 2009), ram pressure stripping (Kapferer et al. 2007) and active galactic nuclei (Moll et al. 2007; Fabjan et al. 2010).

As with early-type galaxies, most of the chemical modelling of the ICM has been done within the monolithic collapse scenario (Matteucci & Gibson 1995; Gibson & Matteucci 1997); although in recent years, several studies have been carried out within the hierarchical assembly paradigm through different model implementations. The various approaches used include semi-analytic models of galaxy formation implemented within merger trees extracted from dissipationless N-body simulations (De Lucia et al. 2004; Nagashima et al. 2005a), full hydrodynamic simulations of cluster formation which include, self-consistently, radiative gas cooling, star formation, feedback and metal enrichment from core collapse SNe and SNe Ia (Valdarnini 2003; Kawata & Gibson 2003a,b; Romeo et al. 2005; Tornatore et al. 2007; Oppenheimer & Davé 2008), and an intermediate hybrid approach that combines N-body and hydrodynamic simulations together with

semi-analytic (or similar) prescriptions of the various physical phenomena (Cora 2006; Cora et al. 2008; Domainko et al. 2006). All these approaches have their own set of strengths and limitations. In the context of SAMs, for instance, De Lucia et al. (2004) assume the instantaneous recycling approximation and trace only the total metallicity and enrichment by type II supernovae (SNe II). Nagashima et al. (2005a), on the other hand, implement detailed galactic chemical evolution models within a SAM and successfully reproduce the abundances of various elements in the ICM, but the same model predicts incorrect trends of stellar abundance ratios in the early-type galaxies within those clusters (Nagashima et al. 2005b). The semi-analytic approach has the advantage of being computationally very cheap, however, this comes at the cost of only predicting global properties given the absence of explicit gas dynamics. On the other hand, hydrodynamic simulations allow the study of the spatial distribution of metals and have been quite succesful at reproducing the observed abundance profiles in clusters. In this case the limitations are that, in hybrid models, the galaxy formation process is not followed in a self-consistent way from the cooling of the gas during the cosmic evolution, and the high computational cost of the fully-consistent simulations. A thourough and complete review on the thermodynamic and chemical properties of the ICM in hydrodynamic simulations can be found in Borgani et al. (2008a,b).

In this work, we make use of the semi-analytic approach combined with detailed galactic chemical evolution models. We have previously shown that our models can reproduce the observed trends for abundances and abundance ratios in nearby early type galaxies in clusters (Arrigoni et al. 2010, hereafter Chapter 2). In this paper we make use of these same models to study the metallicity and abundance ratios of the hot intracluster gas. The outline of the chapter is as follows. In Section 2 we briefly describe the semi-analytic model and the new ingredients. In Section 3 we present our predictions and compare them with observations. In Section 4 we summarise our findings and present our conclusions.

3.2 The semi-analytic model

The backbone of our model is the SAM described by Somerville et al. (2008, hereafter S08), which tracks the hierarchical clustering of dark matter halos, radiative cooling of gas, star formation, SN feedback, AGN feedback (in two distinct modes, quasars and radio jets), galaxy mergers and the starbursts triggered by them, the evolution of stellar populations, and the effects of dust obscuration. In Chapter 2, we described our extension of this model to include detailed metal enrichment by type Ia and type II supernovae and long-lived stars. We refer the reader to the two aforementioned studies for a detailed description of the models.

The SAM has been successful in reproducing a variety of observations in the

local Universe and at high redshift, for example, the luminosity and stellar mass function of galaxies, the colour–magnitude relation, galaxy star formation rates as a function of their stellar masses, the relative numbers of early and late-type galaxies, the gas fractions and size distributions of spiral galaxies, and the global star formation history (S08; Fontanot et al. 2009; Kimm et al. 2009; Hopkins et al. 2009). With the addition of detailed chemical evolution modeling in Chapter 2, the model is able to match the mass–metallicity relation for galaxies and the trend of [α/Fe] with stellar mass, as well as the supernova rates as a function of specific star formation rate (SSFR). To achieve this agreement, it was necessary to adopt a Chabrier IMF (Chabrier 2003) with a slightly flatter slope above 1 $M_\odot$($x = 1.15$ instead of $x = 1.3$), a relatively low fraction of binaries that yield a SN Ia event (0.03 in the $M = 3$–$16\,M_\odot$ range), and a bimodal delay-time-distribution (DTD) with a prompt peak and a later plateau for type Ia supernovae (SNe Ia) explosions, as proposed by Mannucci et al. (2006). We will henceforth refer to the combined GCE plus SAM as the GCE-SAM.

Here we introduce two changes relative to the GCE-SAM described in Chapter 2. First, we have chosen a different set of yields for SNe Ia. Motivated by the excessive amount of Ni present in the galaxies and ISM in Chapter 2, we have switched from the yields of Nomoto et al. (1997, model W7) to those of Iwamoto et al. (1999, model WDD3) as the latter produces only half the Ni while the other elements remain approximately the same. The main difference between these SN models is the scenario for the explosion. The W7 model describes a slow deflagration of the stellar core, while the WDD3 model is calculated using a delayed detonation. The delayed detonation is also the currently favoured SNIa explosion scenario (see, e.g., de Plaa et al. 2007). The yields for SN II and AGB stars remain the same: Woosley & Weaver (1995, hereafter WW95) and Karakas & Lattanzio (2007), respectively.

The other change concerns the immediate fate of the metal-rich gas ejected by the stars. In the "standard" SAM of S08 (as in many SAMs, e.g. de Lucia et al. 2004), these metals were deposited directly in the ISM where it is mixed instantaneously. However, this was a somewhat arbitrary choice. Perhaps a more physical scenario is that the ejecta from massive stars and supernovae, which is highly enriched, is this same material that escapes the galaxy and pollutes the ICM directly. We will use the term "hot enrichment" to refer to this mode of chemical enrichment, in which some fraction of the metals produced and ejected by the stars is deposited directly into the ICM (hot gas phase associated with the dark matter halo) rather than the ISM (cold gas phase associated with the individual galaxy). This picture is supported by observations that indicate that galactic winds are ubiquitously metal-enriched (Martin 2005; Veilleux et al. 2005; Grimes et al. 2009; Weiner et al. 2009), as well as by hydrodynamic simulations of galactic outflows (Mac Low & Ferrara 1999; Madau et al. 2001; Scannapieco et al. 2008). We obtain good results when we assume that 80% of the new metals

are deposited directly in the hot halo gas ($f_{\rm hot\,enrich} = 0.8$).

This scenario has been considered previously by other authors. In the SAM of Nagashima et al. (2005a) the gas and metals ejected by disk stars are deposited in the cold gas in the galaxy, while those from bulge stars are deposited in the hot gas in the halo. In the hybrid model of Cora et al. (2008) half of the mass ejected by stars through stellar winds or supernovae explosions is incorporated directly into the hot phase rather than being first mixed with the cold gas. The latter was done so that the modelled redshift evolution of the mass-metallicity relation resembled the observed one (Erb et al. 2006). More recently, Li et al. (2010) found that if 95% of the newly produced metals are ejected directly into the hot phase for galaxies with a DM halo mass of $5 \times 10^{10} {\rm M}_{\odot}$ or less, their semi-analytic model produces a good match for the mass function and metallicities of the Local Group dwarf satellite population. However, our results indicate that such a mass threshold is not necessary for reproducing the metal abundances in the ICM.

As mentioned before, other possible mechanisms for the enrichment of the ICM include the outflow of metals as a consequence of AGN-driven galactic scale winds. For intance, Fabjan et al. (2010), through AGN feedback, obtain iron abundance profiles with the correct shape, although their normalization is generally higher than observed. In our models, however, the metals (in fact, all the gas) ejected by the AGN-driven winds are assumed to escape the halo entirely because of the high velocities of the winds. Nonetheless, even if all the gas ejected by these winds were retained by the hot halo, the metallicity of the ICM would increase only by 0.05 dex. In our models, the principal effect of the AGN feedback is to prevent cooling onto massive galaxies at low redshift by injecting energy into the ICM through the radio-mode. The mass ejected by the QSO-phase winds is very small.

In this chapter, we adopt a flat ΛCDM cosmology with $\Omega_0 = 0.28$, $\Omega_\Lambda = 0.72$, $h \equiv H_0/(100\,{\rm km\ s^{-1}Mpc^{-1}}) = 0.701$, $\sigma_8 = 0.812$, and a cosmic baryon fraction of $f_b = 0.1658$, following the updated values of the cosmological parameters from Komatsu et al. (2009). We also leave the values of the free parameters associated with the galaxy formation model fixed to the fiducial values given in Chapter 2. We check that these parameters still produce good agreement with our calibration observations in the new "hot enrichment" models in Section 3.3.3.

3.3 Results

In this section, we present our model results for the abundance ratios and metallicities of the ICM, as well as some basic properties of clusters, and compare them with a variety of observations. The simulations were run on a grid of DM halos

* with virial mass ranging from $10^{14.25}\mathrm{M}_{\odot}$ to $10^{15.6}\mathrm{M}_{\odot}$ at an output redshift of $z = 0.05$. This value was chosen because it is the mean redshift of the groups and clusters in the observational samples.

3.3.1 Cluster masses, temperatures and gas fractions

In the observations, clusters are characterised by the measured spectroscopic X-ray temperature. In the models, the ICM temperature is taken to be equal to the halo virial temperature. Assuming isothermality, this temperature relates to the virial velocity as

$$T_{\rm vir}[\mathrm{keV}] = 35.9 k_B (V_{\rm vir}[\mathrm{km/s}])^2, \tag{3.1}$$

where k_B is the Boltzmann constant. At redshift $z = 0.05$, for the chosen cosmology, the previous formula translates to $T_{vir} = 4.12(M_{\rm vir}/10^{15}\mathrm{M}_{\odot})^{2/3}\,\mathrm{keV}$. The virial temperature is, however, systematically lower than the X-ray spectral temperature computed from the data (by typically 10%, Bower et al. 2008). This small correction should not pose an issue in the present work since the predicted and observed chemical properties of the ICM show an extremely flat dependence on cluster temperature.

Before looking into the metal abundances and ratios, we study the total mass and baryonic content of the simulated clusters. In Figure 3.1 we show the virial mass and the hot gas mass fraction of our simulated clusters as a function of temperature. The data points are taken from Reiprich & Böhringer (2002) for the total mass, and Lin et al. (2003); Vikhlinin et al. (2006) and Sun et al. (2009) for the gas fraction. We do not show the models with "hot enrichment" here since this affects only the metal content and has a negligible effect on the total gas mass. In both cases, the models are in qualitative agreement with the data, albeit with some discrepancies. The small difference in the slope of the mass-temperature relation arises because real clusters are not strictly isothermal, as the models assume. Furthermore, correcting for the 10% systematic offset due to using the virial temperature rather than the X-ray temperature would bring the models into better agreement with the data. The hot gas fraction ($M_{\rm hot}/M_{\rm vir}$), however, shows no dependence with temperature over this range, unlike the data, which shows a mild trend of increasing baryonic fraction with temperature. This behavior was already seen in S08 (their Figure 8). Bower et al. (2008) have shown that if "radio mode" AGN feedback not only prevents the cooling of gas but is also allowed to eject some of the hot gas out of the halo, lower-mass clusters in the models will also show lower gas fractions. It is worth noting that our models agree well with the *mean* gas fraction of the entire data sample and that

* The merger trees for each DM halo in the grid are generated before-hand via Monte Carlo realizations according to the extended Press-Schechter formalism. The SAM, which contains all the baryonic physics, is then coupled to these merging trees.

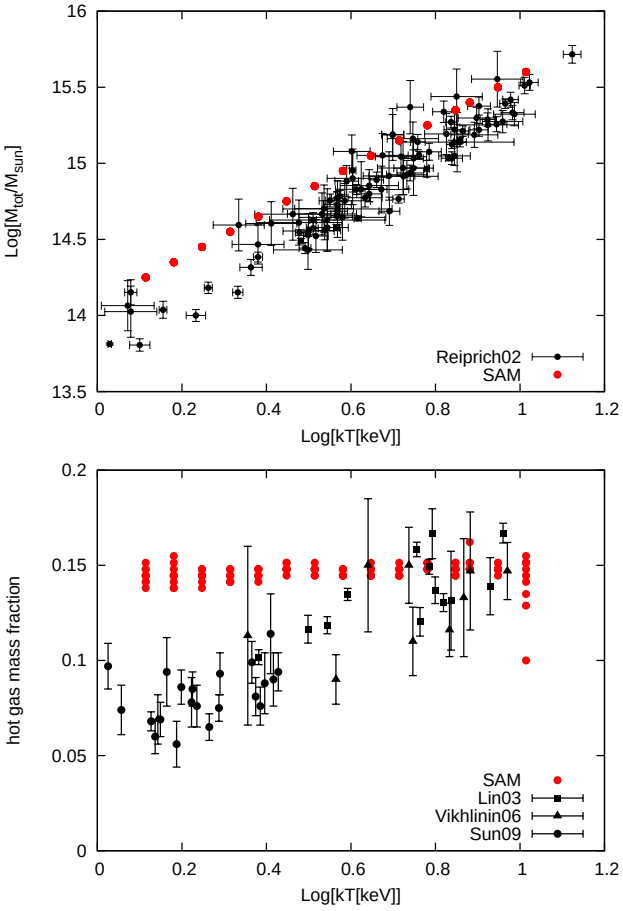

Figure 3.1: *Top:* The virial mass–temperature relation for large groups and clusters. Red circles: Model; black crosses: data points from Reiprich & Böhringer (2002). *Bottom:* The relation between the baryonic mass fraction and temperature. Red circles: Model; black triangles: data points from Vikhlinin et al. (2006); black squares: data points from Lin et al. (2003); black circles: data points from Sun et al. (2009).

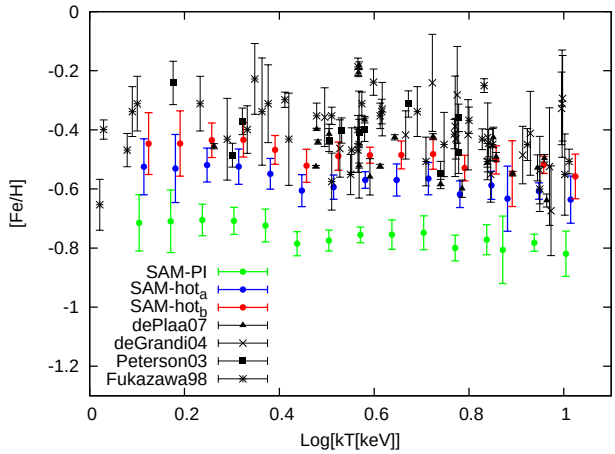

Figure 3.2: Iron abundance in the ICM as function of temperature. Green circles: Chapter 2 fiducial model; blue and red circles: "hot enrichment" models with $A = 0.03$ and $A = 0.04$ respectively; black squares: data points from Peterson et al. (2003); black triangles: data points from de Plaa et al. (2007); black stars: data points from Fukazawa et al. (1998); black crosses: data points from De Grandi et al. (2004). The errorbars on the observational data represent uncertainties, while for the models they indicate the mean and 1σ dispersion over different halo realizations.

model halos below 1 keV ($M_{\rm vir} \sim 10^{12}{\rm M}_{\odot}$) show a sudden drop in the predicted gas fraction (see S08 Figure 8). This step-like behaviour in the gas fraction is common to other models (De Lucia et al. 2004; Menci et al. 2006), and is due to the rapid transition from infall-limited cooling (sometimes called "cold mode") to cooling-time limited cooling ("hot mode").

3.3.2 Metallicities and abundance ratios

Our model proved in Chapter 2 to be successful at reproducing the metallicity- and [α/Fe]-mass relations of local early-type galaxies, as well as the SN rates as a function of SSFR. We now examine the iron content and the abundance ratios between different elements and Fe in the ICM to further test its accuracy. We use an ensemble of X-ray cluster surveys for this purpose. From Fukazawa et al. (1998) we take Si and Fe; from Peterson et al. (2003) we take O, Ne, Mg, Si and Fe; from De Grandi et al. (2004) we take Fe (see also Ettori et al. 2002); and from de Plaa et al. (2007) we take Si, S, Ar, Ca, Fe and Ni. Galaxy clusters often show metallicity gradients for some elements, with increasing abundances towards the cluster centre. These clusters, known as *cool core* (CC) clusters, are mostly relaxed systems and the central metal enhancement is associated with feedback

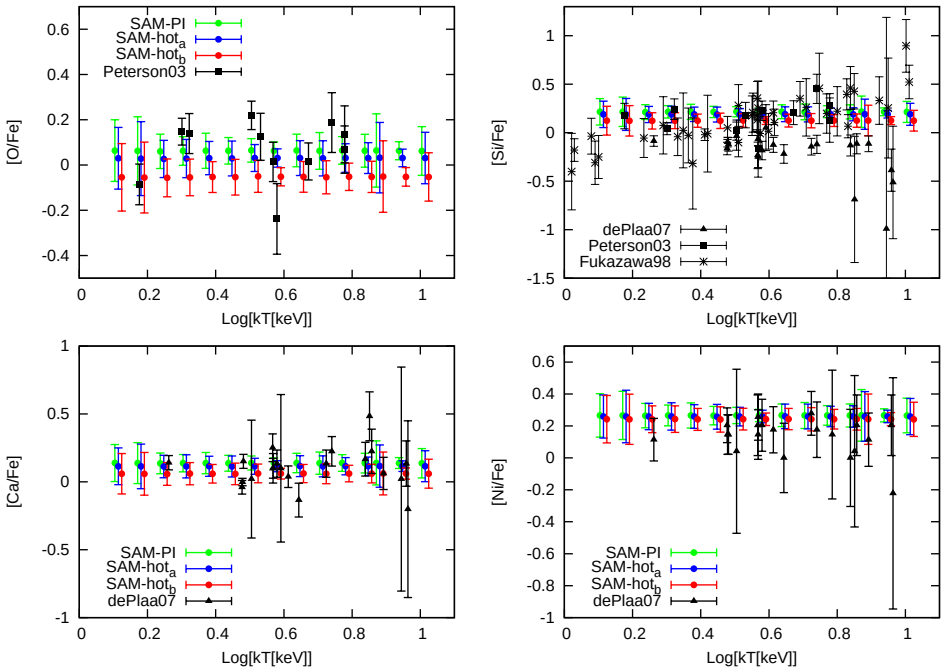

Figure 3.3: Abundance ratios in the ICM as function of temperature, for ratios matched well by the models. Clockwise from top left: [O/Fe], [Si/Fe], [Ni/Fe] and [Ca/Fe]. Symbols as in Figure 3.2. The errorbars on the observational data represent uncertainties, while for the models they indicate the mean and 1σ dispersion over different halo realizations.

from the BCG. This feedback is complemented by the action of AGN-induced buoyant bubbles that have mixed the metals into the ICM, as suggested by Rebusco et al. (2005) and Roediger et al. (2007) in order to explain the observed difference between the broad ICM metallicity profiles and the much narrower stellar light profile of the central galaxy. In addition, low entropy gas enriched at higher redshifts that sinks into the cluster center may also contribute to the central peak of the abundance profile (Cora 2006). In contrast, *non-cool core* (NCC) clusters have almost flat abundance profiles and show signatures of recent merging events (De Grandi & Molendi 2001). Since the observational data are measured near the clusters centres and our models predict global abundances averaged over an entire cluster, it is necessary to correct the observations for gradients, but only for those clusters tagged as having *cool cores*. We do this by following the procedure of Nagashima et al. (2005a, Appendix A), who used the results of De Grandi et al. (2004) on Fe gradients to convert the measured central Fe abundance to global average values. Elements like Si, S, Ar, Ca and Ni are known to have the same gradients as Fe, and are corrected by the same factor; on

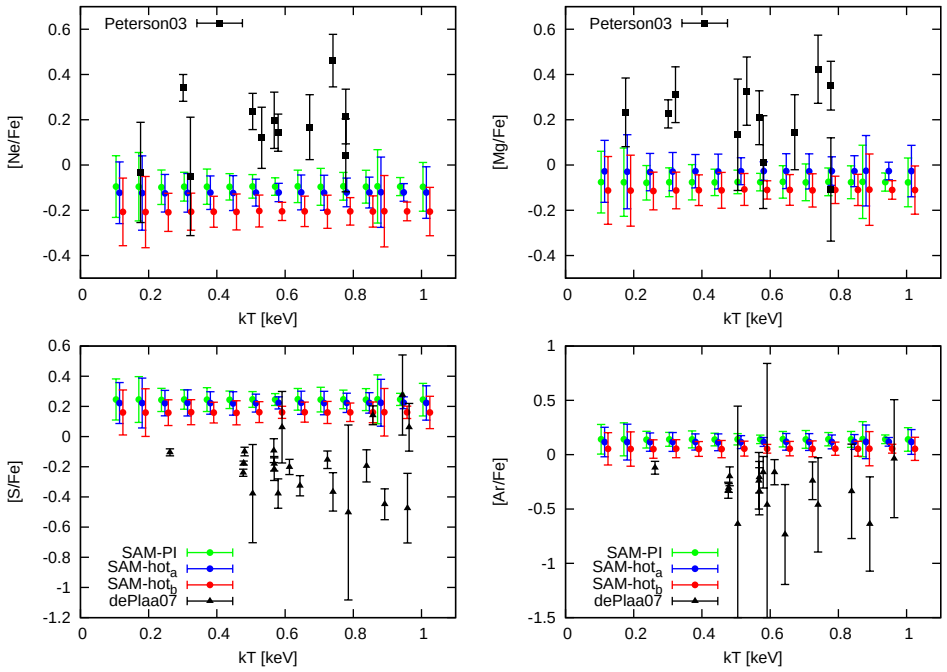

Figure 3.4: Abundance ratios in the ICM as function of temperature, for ratios matched poorly by the models. Clockwise from top left: [Ne/Fe], [Mg/Fe], [Ar/Fe] and [S/Fe]. Symbols as in Figure 3.2. The errorbars on the observational data represent uncertainties, while for the models they indicate the mean and 1σ dispersion over different halo realizations.

the other hand, O, Ne and Mg do not show gradients even in CC clusters, so we assume that the global abundance is equal to the central measurement (Tamura et al. 2001, 2004; Sato et al. 2008, 2009). We have also renormalised the abundances to the solar values of Grevesse et al. (1996), as in the models. Finally, we would like to remind the reader that all values presented in this chapter are abundances by mass.

We will use three different model versions in our comparison: the fiducial model from Chapter 2 (SAM-PI) and two "hot enrichment" models with different values for A (the fraction of binaries that yield a SNIa event). SAM $-$ hot$_a$ uses $A = 0.03$ (the fiducial value adopted in Chapter 2), while SAM $-$ hot$_b$ has a slightly higher value of $A = 0.04$. In Figure 3.2, we examine the elemental abundance of iron ([Fe/H]). We pay particular attention to Fe because it is the ICM element most precisely measured and most extensively studied. Both the data and the models show a flat behaviour with temperature, an effect also seen in the abundance ratios (see below). It is clear that in the original model, the iron abundance is too low and inconsistent with the observations. Depositing the

metals directly into the hot halo gas (hot enrichment) appears to be a plausible solution, bringing the models into marginal agreement with the data. In the models presented here, we have set the fraction of metals deposited directly into the ICM to 80% ($f_{\rm hot\,enrich} = 0.8$). The metallicity of the hot gas depends weakly on this parameter, incresing by about a factor 1.5 over the full parameter range (zero to one).Therefore such a high value for $f_{\rm hot\,enrich}$ is necessary to have a significant effect. In this sense, also, further increasing its value beyond $\simeq 0.75$–0.8 only raises the predicted abundances by a negligible amount. Another way to increase the iron content is by changing the number of type Ia supernovae by adjusting the parameter A, which sets the fraction of binaries that give rise to a SN Ia event. We see that indeed, a higher fraction of type Ia SN binaries provides a better match to the ICM iron abundances, however the value of this parameter is constrained by the observed SN rates and can not take arbitrarily high or low values. As we show later, a binary fraction of 0.04 is still consistent with SNe Ia rates as a function of SSFR for galaxies in the local Universe while producing ICM [Fe/H] abundances that are in marginal agreement with the observed values.

In Figures 3.3 and 3.4 we show the abundance ratios of different elements to iron (O, Ne, Mg, Si, S, Ar, Ca and Ni) in models with and without "hot enrichment". For those with "hot enrichment" we again explore two different values for the SNIa binary fraction, $A = 0.03$ (SAM $-$ hot$_{\rm a}$) and $A = 0.04$ (SAM $-$ hot$_{\rm b}$). There are two aspects that are common to all the elements. Firstly, models with hot enrichment show slightly lower abundance ratios than the standard model, especially for α elements. Secondly, all of the model abundance ratios show a flat behaviour with temperature, as does the data, although the zero point may disagree in some cases. Some of the ratios ([O/Fe], [Si/Fe], [Ca/Fe] and [Ni/Fe]) show a very good match to the observations. On the other hand, the predicted values of [Mg/Fe] and [Ne/Fe] are too low, while [Ar/Fe] and [S/Fe] are overpredicted.

The effect of the higher SNIa binary fraction is naturally stronger on those elements produced mostly by SNII. With the higher [Fe/H] required for a consistent iron abundance, the ratios [Ne/Fe] and [Mg/Fe] are even lower and depart further from the observations. [O/Fe] also decreases but is still consistent. [Ar/Fe] and [S/Fe] are closer to the data but are still overpredicted and only marginally consistent with the observations. [Si/Fe] and [Ca/Fe] remain in good agreement. Finally, [Ni/Fe] shows no variation with the binary fraction parameter A, which is reassuring as both elements are predominantly produced by SNIa.

In the case of [Mg/Fe], the model ratios can be raised by increasing the Mg yield in stars above 20 $M_\odot$, a common practice with the WW95 yields (see, e.g., François et al. 2004). In Chapter 2 there was no need for such a modification, but in this case increasing the Mg yield by a factor of 2.5 brings the ICM abundance ratio into good agreement with the data, while still maintaining an observationally

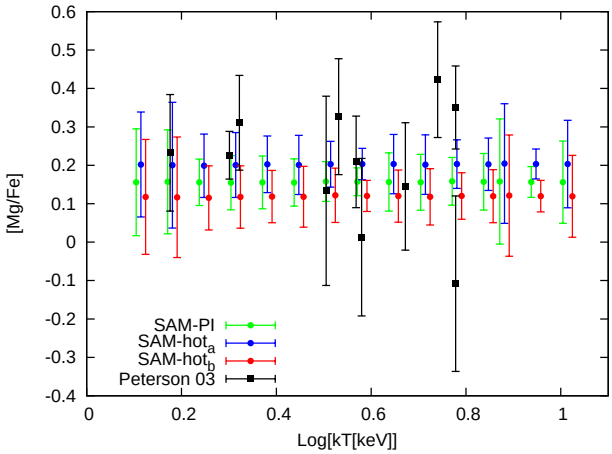

Figure 3.5: [Mg/Fe] in the ICM as a function of temperature for models with the magnesium yield from SNII increased by a factor 2.5. Symbols as in Figure 3.2. The errorbars on the observational data represent uncertainties, while for the models they indicate the mean and 1σ dispersion over different halo realizations.

consistent [Mg/Fe] in the galaxies' stellar component. * A slightly higher factor would give a better match for the ICM, but in that case the stellar abundance ratios would be too high. Models with a boosted magnesium yield are shown in Figure 3.5. In principle, the same exercise could be done with the yields of other elements that are underpredicted (Ne) or overpredicted (Si, Ar). However this should not be considered a solution, but simply a tentative constraint on nucleosynthesis from the chemical evolution models. Also, we have assumed that the different elements in the ICM either have no radial gradients at all or that they have the same gradient as iron (for which there are fairly good measurements). This simple assumption might not be strictly true and a more accurate correction for gradients could bring the models and the data into better agreement. Future observations of gradients of elements other than iron in the ICM would shed some light on this matter.

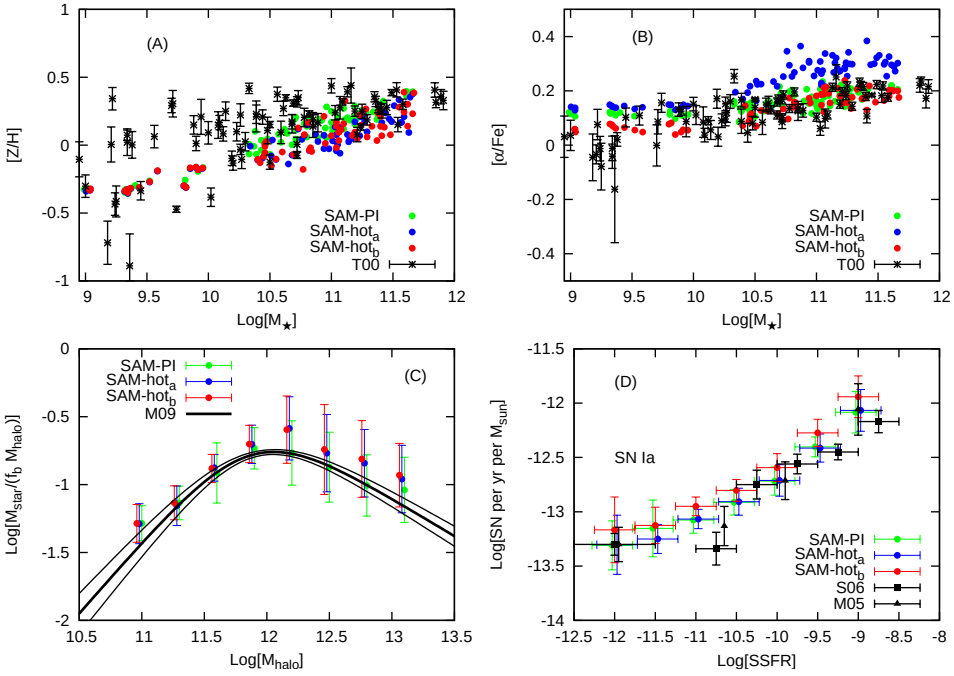

Figure 3.6: Predicted properties of galaxies in the local Universe. Clockwise, starting from the top left panel: (A) [Z/H] vs. stellar mass for early-type galaxies; (B) [α/Fe] vs. stellar mass for early-type galaxies; (C) Type Ia SNR vs. SSFR; (D) Fraction of baryons in the form of stars as a function of halo mass. Symbols – green circles: Chapter 2 fiducial model; blue and red circles: "hot enrichment" models with $A = 0.03$ and $A = 0.04$ respectively; T00: reanalysed metallicities and abundance ratios from Trager et al. (2000a) as presented in Chapter 2; M05 and S06: SN rates from Mannucci et al. (2005) and Sullivan et al. (2006) respectively; M09: the empirical relation, and 1σ uncertainties, derived by Moster et al. (2009).

3.3.3 Effects of "hot enrichment" on galaxy properties

We have introduced a fairly significant modification to our model — the deposition of the majority of the newly produced metals into the hot halo gas, instead of into the cold interstellar gas. It is important to check whether this change has an impact on the properties of galaxies that we used to calibrate our previous models. In Figure 3.6 we show the same three models as in the previous section (Chapter 2 fiducial, SAM-PI; hot enrichment with $A = 0.03$, SAM $-$ hot$_{\rm a}$; and hot enrichment with $A = 0.04$, SAM $-$ hot$_{\rm b}$). We show the metallicity, [α/Fe] ratio, SN Ia rate of galaxies and the fraction of baryons in the form of stars as a function of halo mass, and compare them with the same data samples from the local Universe as in Chapter 2. We remind the reader that the fiducial model from Chapter 2 had $A = 0.03$.

The metallicities of early-type galaxies are not significantly affected by this change and remain in agreement with the observations (panel A). However, galaxies in models with "hot enrichment" have their [α/Fe] increased (especially the most massive galaxies). A higher value of the binary fraction parameter A brings the abundance ratios back into agreement with the observations (panel B). From panel (C) in Figure 3.6, we see that the lower value of $A = 0.03$ provides a better fit to the SN Ia rates as a function of the specific star formation rate (SSFR), although a value of $A = 0.04$ is still consistent with the data. Considering that a higher fraction of stars that explode as SNe Ia is also required to make the iron content in the ICM consistent with the data, $A = 0.04$ gives a better overall agreement between the models and the observations.

Another concern is that when metals are deposited directly into the hot gas, elevating the metal content, the cooling rate increases, possibly resulting in the conversion of a larger fraction of the baryons in the halo into stars. This could result in the production of an overabundance of massive galaxies relative to observations. We check this by investigating the ratio of the mass of baryons that have turned into stars in the central galaxy to the mass of baryons that would be contained in the halo in the absence of star formation or feedback (i.e. $f_{\rm b} M_{\rm vir}$, where $f_{\rm b}$ is the universal baryon fraction), as a function of halo mass. We compare the model predictions with the empirical constraint from Moster et al. (2009), which is derived by requiring that the observed stellar mass function is reproduced for a given assumed multiplicity function of dark matter halos (i.e. as predicted by

* The stellar [Mg/Fe] increases by about 0.66 dex at M*$\sim 10^{9}$M$_{\odot}$and 0.4 dex at M*$\sim 10^{11.5}$M$_{\odot}$. But in terms of [α/Fe] the increment is much smaller, only 0.12 dex at M*$\sim 10^{9}$M$_{\odot}$and 0.08 dex at M*$\sim 10^{11.5}$M$_{\odot}$. This is at a fixed SN Ia fraction. It is also important to remember that the preferred "hot enrichment" model has a higher A value than the fiducial model from Chapter 2, and therefore higher Fe abundances in all the barionic components. The net effect of increasing both the Mg yield and the fraction of SNIa binaries is reduced: [Mg/Fe] increases by 0.52/0.25 dex while [α/Fe] decreases by -0.001/-0.04 dex (at M*$\sim 10^{9}$M$_{\odot}$and $10^{11.5}$M$_{\odot}$respectively).

a given ΛCDM model). As we can see from panel (D) in Figure 3.6, the effect of the new model ingredients is small and all models are consistent with each other and with the data.

3.4 Discussion and Conclusions

We have investigated the metal enrichment of the intracluster medium within the framework of hierarchical assembly using the same model presented in Chapter 2, which successfully reproduces the abundance ratios of early-type galaxies in the local Universe by assuming a slightly flat IMF ($x = 1.15$) and a bimodal Delay-Time-Distribution of type Ia supernovae.

Our most important finding is the need for some form of metal enriched outflows from galaxies because the ICM iron abundance is too low otherwise. Adopting "hot enrichment", in which 80% of the metal-rich material ejected by the stars is deposited directly into the ICM rather than the ISM, seems to be a reasonable solution. This type of metal enhanced galactic winds is in agreement with previous works (Portinari et al. 2004; Cora et al. 2008; Sivanandam et al. 2009). We also need slightly more type Ia supernovae, both for the iron in the ICM and the [α/Fe] in the galaxies. Although the fit to SNR vs. SSFR is not as good as in Chapter 2, it is still consistent with the observations.

Regarding the elemental abundance ratios in the ICM, the models predict flat behaviour with cluster temperature, in agreement with the observations. For some elements (O, Si, Ca, Ni) the zero-point is reproduced remarkably well, while others agree only marginally (Ar, S), or are significantly underpredicted (Ne, Mg). This occurs irrespective of whether "hot enrichment" is assumed or not. The [Mg/Fe] can be fixed by increasing the Mg yield in SN II (as is commonly done with the WW95 yields). The discrepancy in the other elements may arise from uncertainties in the yields and/or the correction for radial gradients (we assume that elements that have a gradient share the same one as Fe, which might not be strictly correct, although they cannot be too different).

Overall the model *simultaneously* produces acceptable predictions for the chemical properties of galaxies in the local Universe and the ICM in nearby clusters. This is yet another step forward in building a self-consistent framework for predicting the properties of diverse populations within the context of the hierarchical galaxy formation framework.